Optica Applicata, Vol. XLVI, No. 2, 2016
DOI: 10.5277/oa160213

Method for improving sinusoidal quality of error diffusion binary encoded fringe used in phase measurement profilometry

ZIXIA TIAN, WENJING CHEN*, XIANYU SU

Opto-Electronic Department, School of Electronic and Information Engineering, Sichuan University, Chengdu, Sichuan 610064, China

*Corresponding author: chenwj0409@scu.edu.cn

Insufficient resolution of digital-light-processing projector will degrade the sinusoidal quality of the binary encoded fringe pattern because of less sampling points in a fringe period, which will degrade the measurement accuracy if it is used in phase measurement profilometry. Two resolutions are proposed in the paper. One is that a cylindrical lens is introduced in the projecting light path of the measurement system to improve sinusoidal quality of the binary encoded fringe by elliptical low-pass filtering of the system. The other one is that superposition of multi-frame binary encoded gratings with different microstructure is to reduce the binary image noise for improving the measurement accuracy. Simulations and experiments verify the validity of the above two methods.

Keywords: phase measurement profilometry, digital-light-processing (DLP) projector, error diffusion algorithm, binary encoded grating.

1. Introduction

With the development of digital video projection technology, 3D shape measurement techniques based on the digital fringe projection have drastically improved [1–3], especially the dynamic high-speed 3D shape measurement [2, 4]. However, a commercial digital video projector suffers from the major limitations of speed bottleneck (typically 120 Hz) and projection nonlinearity [2].

The recently proposed binary defocusing technique [5] could not only overcome speed bottleneck and projection nonlinearity of digital-light-processing (DLP) projector by taking advantage of the fast binary image switching functionality. However, if the measurement depth is large and the high measurement speed is required, the measurement accuracy will be limited because of the existence of the high-frequency harmonics in the binary encoded fringe [6].

1D pulse width modulation (PWM) techniques [7–9] and 2D area modulation technique [10, 11] have been studied to improve the measurement accuracy for the high-order harmonics being shifted further away from fundamental frequency or being

eliminated. However, the PWM techniques can generate high-quality sinusoidal fringe patterns only when the fringe stripes are narrow [8]. For a digital video projector, it is difficult for 2D area modulation techniques proposed in [10] to generate high quality fringe pattern when fringe stripes are wide, while the 2D area modulation techniques proposed in [11] cannot generate high quality area modulation grating because of the insufficient resolution of the DLP projector.

The grating generated by the error diffusion algorithm has numerous merits over the squared binary defocusing method and pulse width modulation method [12–16]. But more than 100 pixels in a fringe period are needed for guaranteeing a good quality sinusoidal grating to be obtained [17–20].

However, many commercial DLP projectors have about 1024×768 pixels resolution, and the binary sampling points are far less than 100 pixels in a fringe period if the high density fringe meeting the measurement requirement is projected. For example, projecting 60 stripes, the sampling number is less than 20 pixels in a fringe period. Some optimization algorithms, such as genetic algorithm [17], optimization based on the symmetry and periodicity [18], phase optimization [19] and intensity optimization [20] have been employed to improve the grating quality. However, genetic algorithm is very time-consuming; optimization through symmetry and periodicity may generate two similar local patterns that need to be judged artificially which one is chosen to generate the whole pattern.

For high-speed 3D shape measurement, the phase measuring profilometry (PMP) based on the binary sinusoidal fringe projection and less-step phase shifting algorithm is popular, in which, the phase accuracy is not only decided by the sinusoidal quality of the binary fringe pattern, but, on the other hand, also is used to describe the sinusoidal quality [17–19].

Two resolutions are proposed to improve the sinusoidal quality of the binary encoded fringe (BEF). A cylindrical lens can be introduced in the light path to form an elliptical low-pass filter. The other one is that multi-frame binary encoded gratings with different microstructure are superposed to reduce the error of the binary encoded fringe. Especially when the sampling numbers in a fringe period are small, the two proposed methods can greatly improve the measurement accuracy of PMP based on binary encoded fringe projection. Both simulations and experiments verify the validity of the above two methods.

Section 2 explains the principle of the phase-shifting algorithm and the error diffusion dithering technique. Section 3 explains the proposed two methods. Section 4 shows the simulation results. Section 5 presents the experimental results, and finally Section 6 summarizes this paper.

2. Principle

2.1. Four-step phase-shifting algorithm

Phase-shifting techniques have been extensively used in optical metrology because of high accuracy [21, 22]. The more fringe patterns used, the higher measurement accu-

racy can be achieved. The four-step phase-shifting algorithm is less sensitive to surface reflectivity variations. The third order harmonics in the fringe and ambient light will be used in this paper. Four fringe images applied in the four-step phase-shifting algorithm can be described as:

$$I_1(x, y) = a(x, y) + b(x, y)\cos[\phi(x, y)] \tag{1}$$

$$I_2(x, y) = a(x, y) + b(x, y)\cos[\phi(x, y) + \pi/2] \tag{2}$$

$$I_3(x, y) = a(x, y) + b(x, y)\cos[\phi(x, y) + \pi] \tag{3}$$

$$I_4(x, y) = a(x, y) + b(x, y)\cos[\phi(x, y) + 3\pi/2] \tag{4}$$

where $a(x, y)$ and $b(x, y)$ are the background and the contrast, respectively, and $\phi(x, y)$ is the phase. Simultaneously solving Eqs. (1)–(4), the phase can be obtained as

$$\phi(x, y) = \tan^{-1}\left[\frac{I_4(x, y) - I_2(x, y)}{I_1(x, y) - I_3(x, y)}\right] \tag{5}$$

and $\phi(x, y)$ ranges from $-\pi$ to $+\pi$ with 2π discontinuities. A continuous phase map can be obtained by adopting a suitable phase unwrapping algorithm [23].

2.2. Error-diffusion dithering technique

In error-diffusion algorithm, the pixels are quantized in specific order, and the quantization error for the current pixel is propagated forward to local unprocessed pixels through the following equation:

$$\tilde{I}(i, j) = I(i, j) + \sum_{k, l \in S} h(k, l)e(i - k, j - l) \tag{6}$$

where $I(x, y)$ is the original image, $\tilde{I}(x, y)$ is the quantized image, and quantization error $e(i, j)$ represents the difference between the quantized image pixel and the diffused image pixel; $e(i, j)$ is further diffused to its neighboring pixels through 2D diffusion kernel function $h(k, l)$; S represents the zone of the unprocessed pixels. In this paper, the serpentine raster [15] Sierra Lite error diffusion encoded algorithm is used to generate the binary encoded fringe pattern. The diffusion kernels are:

$$\text{Odd row:} \quad h(k, l) = \frac{1}{4}\begin{bmatrix} - & x & 2 \\ 1 & 1 & \end{bmatrix} \tag{7}$$

$$\text{Even row:} \quad h(k, l) = \frac{1}{4}\begin{bmatrix} 2 & x & - \\ & 1 & 1 \end{bmatrix} \tag{8}$$

where "–" represents the processed pixel, and x represents the pixel in process [18].

3. Methods for improving the sinusoidal quality of binary encoded fringe

Most commercial DLP projectors have 1024×768 pixels resolution, the binary sampling points are far less than 100 pixels in a fringe period for projecting the fringe meeting the requirement of PMP measurement. In order to keep the measurement accuracy, two improved techniques are introduced.

3.1. Set up a cylindrical lens in the measurement system

Because of the low-pass filtering function of the measurement system, keeping the DLP projector at the focusing state, the projected binary encoded fringe image can be regarded as a convolution result of the ideal binary grating and a point spread function of the projector system, which can be simplified as a small size low-pass Gaussian filter with circular symmetry structure. The low-pass filtering operation of the DLP projector will make the binary encoded fringe be smoothed in the row and column direction equally, and the fringe contrast will be decreased, especially when sampling numbers are less in a fringe period. If a cylindrical lens is set in front of the projection lens, the focus of the imaging system will change in one direction. According to the imaging theory of the cylindrical lens, a point at the object space can "image" a line along the cylindrical lens' meridian plane. It causes the spherical wavefront from the projection lens to become an astigmatic wavefront, and the extended size in meridian direction is larger than that in sagittal direction, as shown in Fig. 1. Therefore, the superposition of the point spread function of the projection lens and the cylindrical lens can be regarded as a low pass filter with elliptical structure under the condition of the geometrical optical approximation, in which the long axis is along the grating line direction and the short axis is perpendicular to the grating line direction. The binary encoded

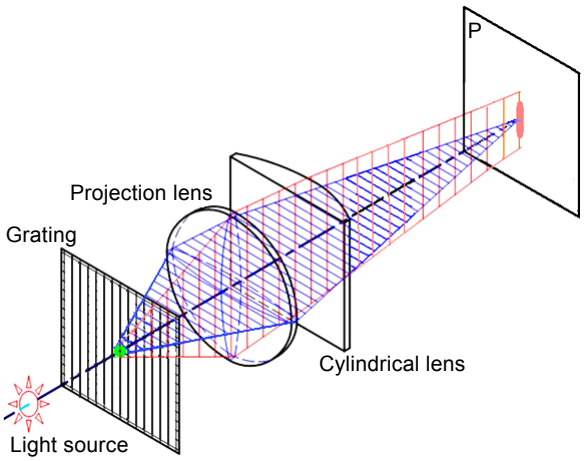

Fig. 1. Function diagram of cylindrical lens.

grating will be blurred less along the short axis direction, which improves the sinusoidal quality of the binary encoded fringe.

However, if the point spread function of the system is elliptical, the long axis is along the grating line direction and the short axis is perpendicular to the grating line direction, and the binary encoded grating will be blurred along the long axis direction much more than along the short axis direction. The pattern will maintain high contrast along the grating line. Setting up a cylindrical lens in front of the projector, the result point spread function has the property of the elliptical symmetry, which will improve the sinusoidal quality of the binary encoded fringe.

3.2. Superposition of multi-frame binary encoded fringe with different microstructures

As it is known the noise standard error $\sigma_{\bar{g}(x,y)}$ of the resulted fringe from the superposition of K-frame images with noise is smaller than that of a single frame image $\sigma_{\eta(x,y)}$, the relationship is as follows:

$$\sigma_{\bar{g}(x,y)} = \frac{1}{\sqrt{K}} \sigma_{\eta(x,y)} \tag{9}$$

The gratings with different microstructures can be generated by different diffusion kernels or by cutting out from a bigger size binary encoded fringe generated by one error defusing algorithm starting in different rows. Figure 2 illustrates zoom-in binary gratings for showing their microstructures when the fringe period $T = 16$ pixels. Figure 2**a** is a part of the binary encoded fringe obtained by Floyd–Steinberg distance weight error diffusion algorithm. Figure 2**b** shows a part of the binary encoded fringe obtained by serpentine raster Sierra Lite error diffusion algorithm. Figure 2**c** is a scheme for selecting multi-frame fringes. Here different color lines denote different starting rows for cutting out the same size binary encoded gratings for superposition from a bigger size binary grating.

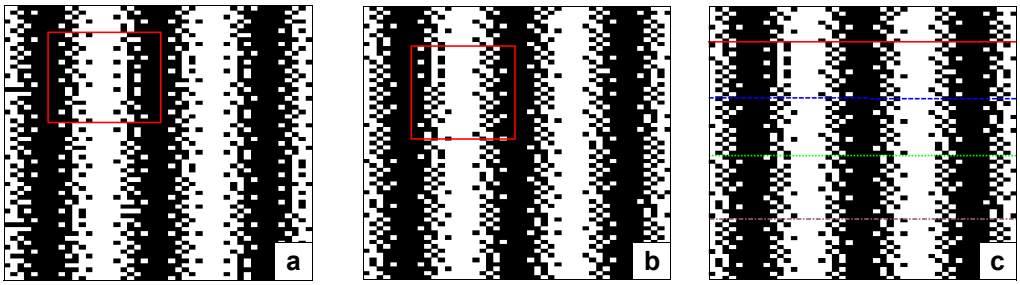

Fig. 2. Zoom-in binary encoded fringe when the fringe period $T = 16$ pixels. The binary encoded fringe obtained by Floyd–Steinberg distance weight algorithm (**a**); the binary encoded fringe obtained by serpentine raster Sierra Lite algorithm (**b**); a scheme for selecting multi-frame fringes (**c**).

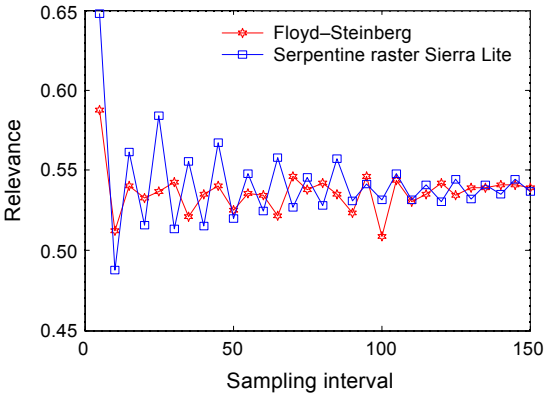

Fig. 3. The correlation result when the fringe period $T = 16$ pixels.

Figure 3 illustrates the correlation analysis curves when the fringe period $T = 16$ pixels with 5 pixels as an interval along the grating line. Two original fringes with the size of 1024×1024 pixels are generated by Floyd–Steinberg distance weight algorithm and serpentine raster Sierra Lite algorithm, respectively. The ups and downs of correlation curve obtained by the serpentine raster Sierra Lite algorithms are a little bigger, but the correlation values in the curves are almost within [0.5, 0.6]. In the simulations and the experiments, the serpentine raster Sierra Lite binary encoded fringes are employed.

4. Computer simulations

Computer simulations are carried out to verify our methods. First, the sinusoidal quality, the intensity errors between the smoothed binary encoded fringe pattern and the ideal sinusoidal grating pattern, are shown in Fig. 4. A very small Gaussian filter (5×5 pixels and standard deviation 5/3 pixels) is used to emulate the low pass filtering property of the both projector and imaging device. When a cylindrical lens is set up in the system, an elliptical Gaussian filter (13×5 pixels and standard deviation 5/3 pixels) is used. Figure 4**a** shows the sinusoidal intensity differences between the binary encoded fringe patterns respectively smoothed by Gaussian filter and elliptical filter and the ideal gray sinusoidal grating pattern when the fringe period $T = 16$ pixels. Figure 4**b** shows the comparison result when the fringe period $T = 60$ pixels. Figures 4**c** and 4**d** show that the sinusoidal quality of the resulted binary encoded fringe patterns is increased by the superposition of the multi-frame binary encoded gratings after adding a cylindrical lens in the optical path.

Figure 5 shows the intensity standard errors and phase standard errors obtained by the proposed methods responding to different fringe periods $T = 10, 16, 30, 40, 50$, and 60 pixels, respectively. Figure 5**a** shows that the sinusoidal error between the binary

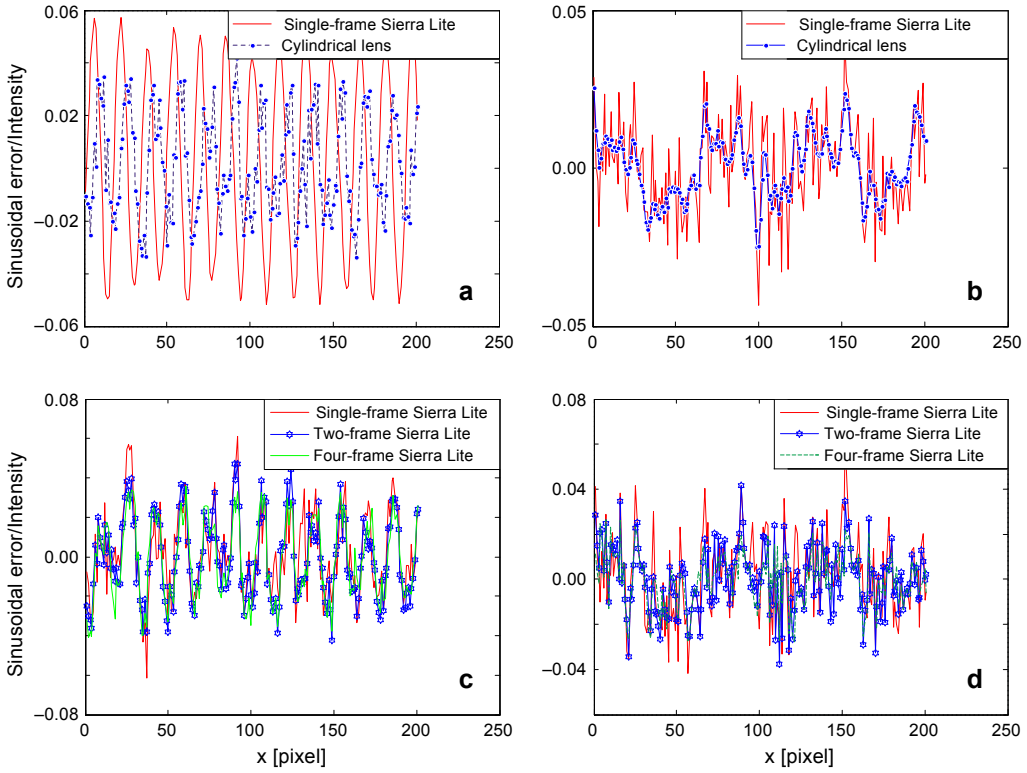

Fig. 4. Sinusoidal intensity errors. Sinusoidal error with or without a cylindrical lens in the optical path when $T = 16$ pixels (**a**) and $T = 60$ pixels (**b**). Sinusoidal errors by superposing multi-frame gratings when $T = 16$ pixels (**c**) and $T = 60$ pixels (**d**).

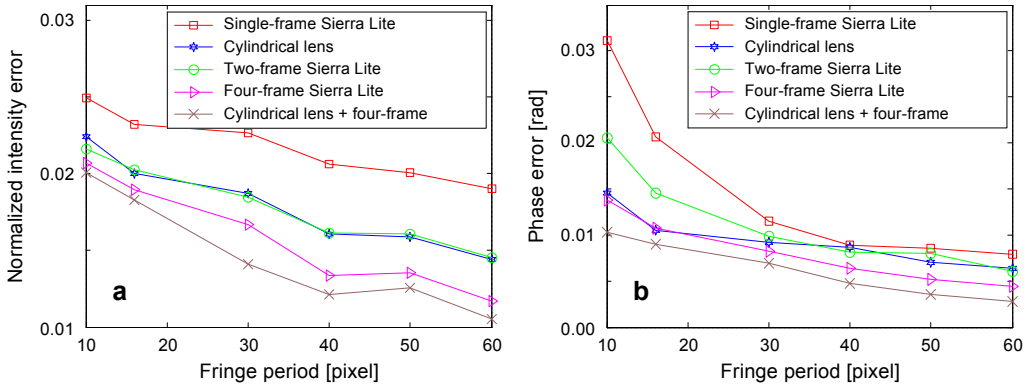

Fig. 5. Intensity standard errors (**a**) and phase standard errors (**b**) of the proposed methods when the fringe periods $T = 10$, 16, 30, 40, 50, and 60 pixels.

encoded fringe pattern and the responding ideal sinusoidal grating pattern is decreased. Figure 5**b** shows that the phase errors calculated by PMP method are decreased as well.

5. Experimental results

We carried out experiments to verify the performance of our proposed methods. Figure 6 is the measurement system including a DLP projector (EPSON EMP-280), a cylindrical lens, a CCD camera (MVCII-1M) and a computer. The resolutions of the projector and CCD are 1024×768 pixels and 1024×1280 pixels, respectively. The dioptric of the cylindrical lens is negative 200 degree. In the experiment, both the projector and CCD were focused. First, a set of fringes with periods T = 10, 16, 30, 40, 50, and 60 pixels are projected on a standard white flat board.

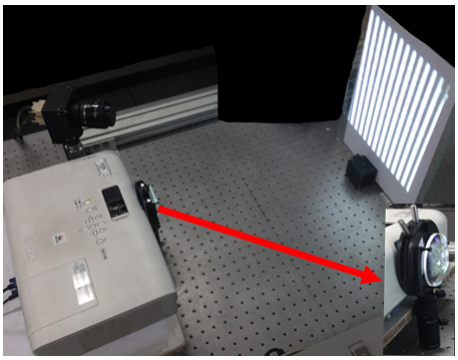

Fig. 6. Diagram of experiment set up.

Figure 7**a** shows a part of the captured binary encoded fringe on cylindrical lens in the measurement system when T = 16 pixels. It clearly shows that there are lots of particles which will introduce high order spectra in the grating pattern and decrease the sinusoidal quality of the grating. Figure 7**b** shows a captured binary encoded fringe with a cylindrical lens in the system keeping other conditions unchanged. Figure 7**c** shows that the intensity standard errors between the binary encoded fringe and the gray sinusoidal grating can be decreased by our methods when fringes with different periods are projected. Figure 7**d** shows that the phase standard errors calculated by PMP method from the binary encoded gratings are decreased after a cylindrical lens is set up in the system.

Figure 8 shows the sinusoidal quality and phase error of the result binary encoded fringe after employing multi-frame superposing and cylindrical lens. Figure 8**a** shows the intensity standard errors between the superposition of the multi-frame binary encoded gratings and the gray sinusoidal grating. Figure 8**b** shows the phase standard error curves calculated from the phase difference between the phase maps demodulated from the single binary encoded fringe, the result of the binary encoded fringe by two-frame gratings superposition, the four-frame gratings superposition, respectively,

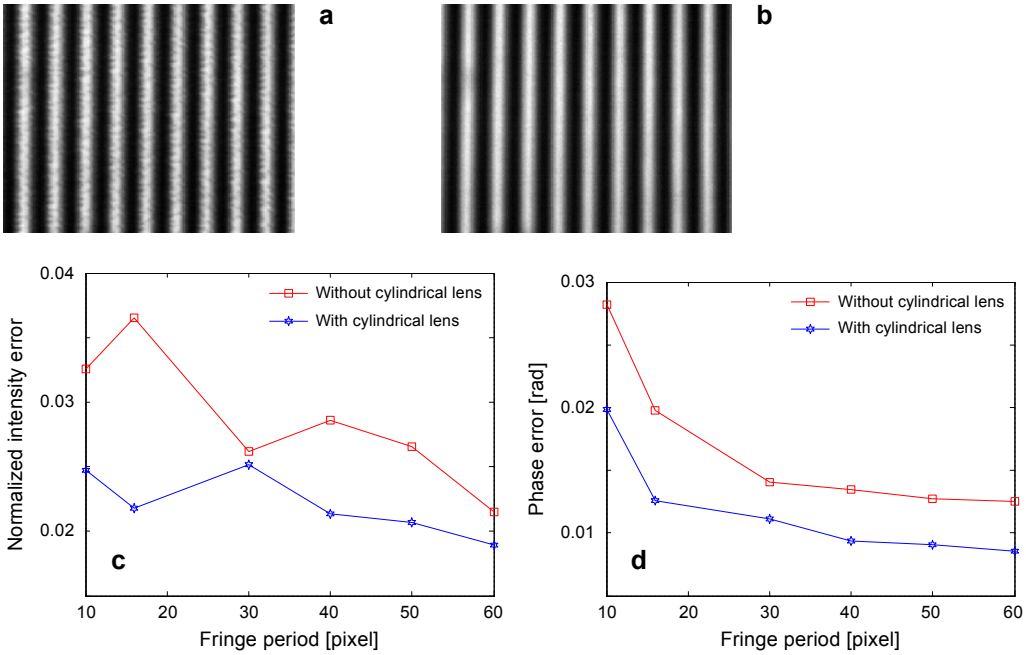

Fig. 7. Binary encoded fringe intensity and errors. Captured binary encoded fringe without (**a**) and with (**b**) cylindrical lens. Intensity standard errors with or without cylindrical lens (**c**). Phase standard errors with or without cylindrical lens (**d**).

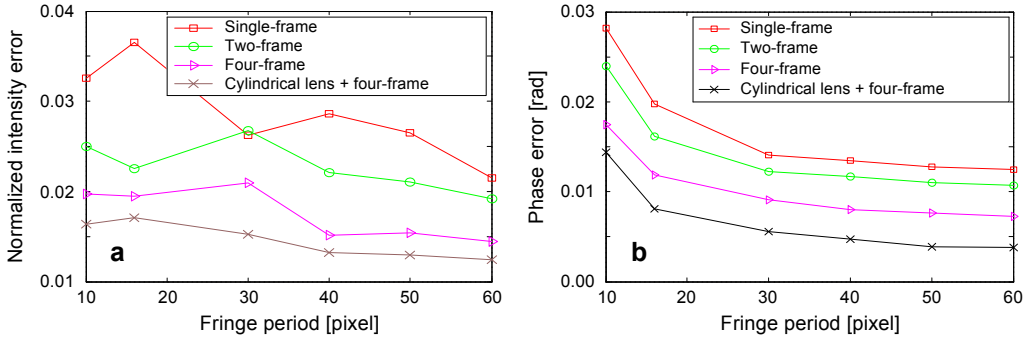

Fig. 8. Sinusoidal quality and phase error. Intensity standard errors (**a**) and phase errors (**b**).

and that of the gray sinusoidal grating by PMP method when $T = 10, 16, 30, 40, 50, 60$ pixels. It also shows that adding a cylindrical lens in the measurement system will bring the improvement of the phase accuracy even when the fringe period is small.

Figure 9 shows the reconstruction of the white board by the PMP method corresponding to the above different conditions. Figure 9**a** shows the 100th row of the reconstructed phase distribution and its local enlarged view from 10th pixel to 20th pixel.

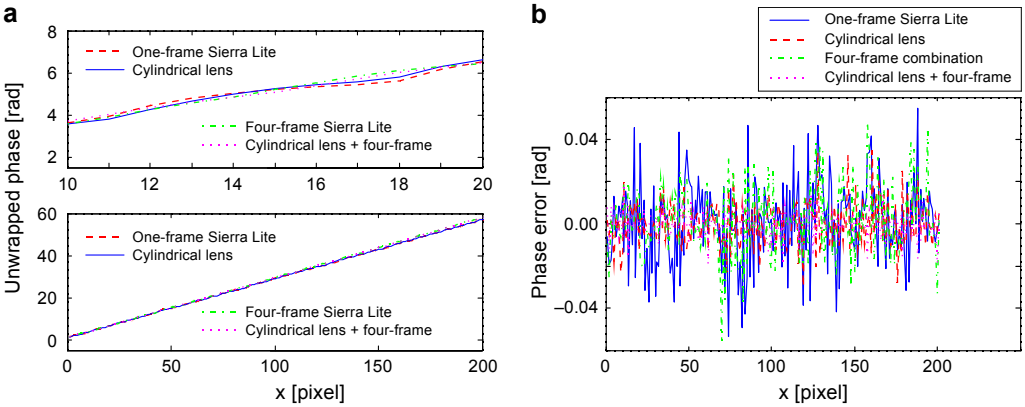

Fig. 9. The reconstructed phase and errors. The 100th row reconstructed phase and its local enlarged view from 10th to 20th pixel (**a**). Phase standard errors between the binary encoded fringes and the ideal sinusoidal fringe (**b**).

Figure 9**b** shows the phase differences between the phases obtained from the binary encoded gratings by the above methods and those from the ideal gray sinusoidal fringe.

Table 1 contains the standard errors and maximum errors obtained by different methods when the fringe period $T = 16$ pixels. Figure 9 and Table 1 show that the combination of the cylindrical lens and superposition of multi-frame gratings can clearly decrease measuring errors.

T a b l e 1. Standard and maximum errors of different methods.

	Methods				
Error	One-frame grating	Two-frame grating	Four-frame grating	Cylindrical lens	Cylindrical lens and four-frame
Standard	0.019753	0.01616	0.0117	0.012567	0.0074814
Maximum	0.11263	0.10132	0.0698	0.08036	0.047493

Another experiment verifies our methods. Figure 10**a** is a captured fringe image with a cylindrical lens in the system. The fringe period $T = 16$ pixels, and the four-steps PMP method is used. Figures 10**b**, 10**c** and 10**d** show the reconstructed phases through adding cylindrical lens in the system, the superposition of multi-frame gratings and the superposition of multi-frame gratings combining cylindrical lens in the system, respectively. For clarity, Fig. 10**e** shows the results of phases of the 400th column of the object by difference methods, including a local enlargement section in the figure. Its shows that by the proposed methods, the phase blurs are obviously reduced.

6. Conclusion

Two methods are proposed to obtain high-quality binary encoded sinusoidal fringe patterns by error-diffusion algorithm when the sampling numbers in a fringe period are

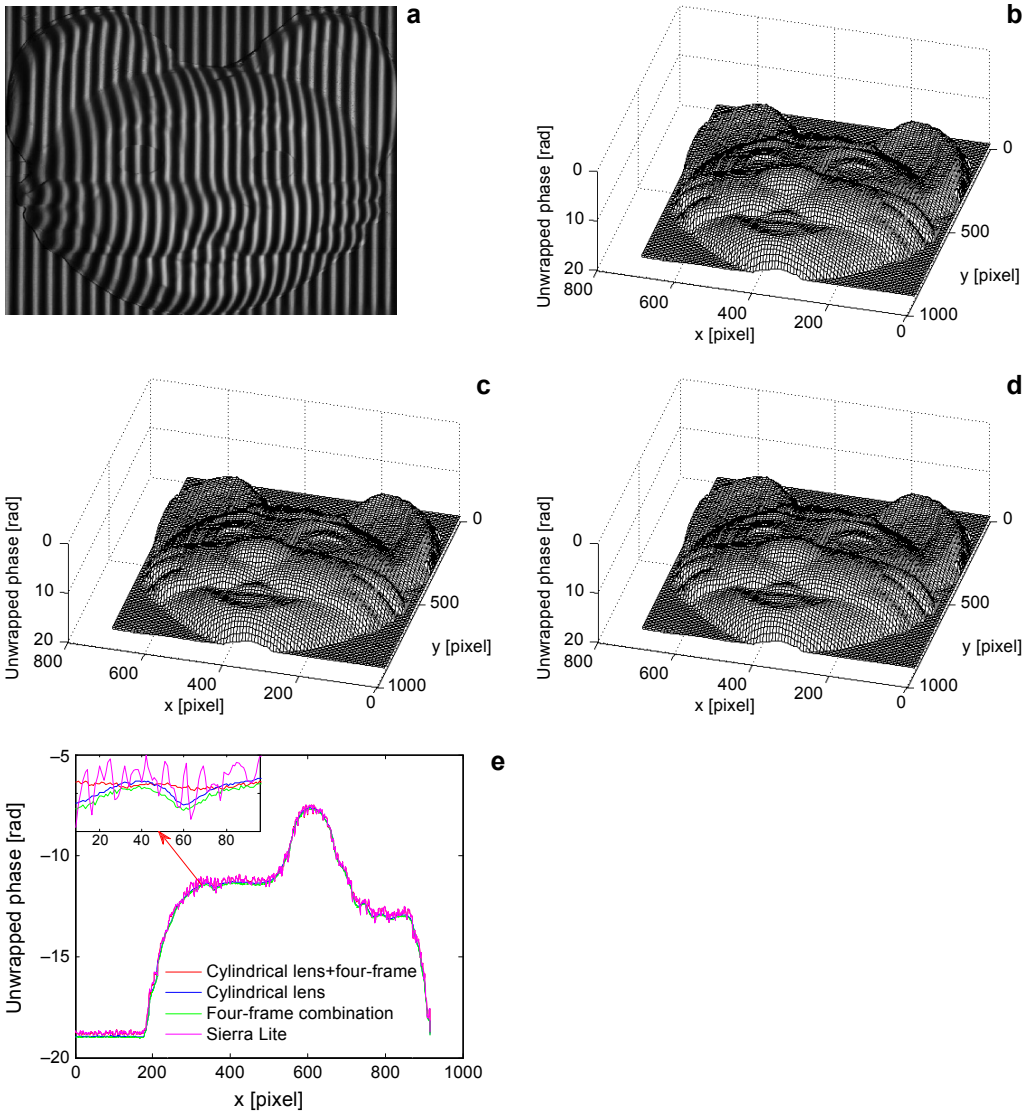

Fig. 10. Measurement results. The deformed binary encoded fringe pattern with cylindrical lens (**a**); the reconstructed phase with cylindrical lens (**b**); the reconstructed phase from the superposition of multi -frame gratings without cylindrical lens (**c**); the reconstructed phase from the superposition of multi-frame gratings with cylindrical lens (**d**); the 400th column of phases by difference methods (**e**).

less than 100 pixels. One is that a cylindrical lens is introduced in the light path of the measurement system to smooth the binary encoded fringe along the grating line direction by elliptical low-pass filtering. The other is that the multi-frame binary encoded sinusoidal gratings with different microstructure are superposed to reduce the noise of the binary encoded fringe and guarantee the measurement accuracy. The combination of the methods can bring better results. Both simulations and experiments verify the

validity of the above methods in improving the sinusoidal quality of the binary encoded fringe and the precision of the PMP method.

Acknowledgments – This work was partially supported by Major National Special Instrument under the project numbers of 2013YQ49087901.

References

[1] CHEN F., BROWN G.M., MUMIN SONG, *Overview of three dimensional shape measurement using optical methods*, Optical Engineering **39**(1), 2000, pp. 10–22.

[2] SONG ZHANG, *Recent progresses on real-time 3D shape measurement using digital fringe projection techniques*, Optics and Lasers in Engineering **48**(2), 2010, pp. 149–158.

[3] GENG J., *Stuctured-light 3D surface imaging: a tutotial*, Advances in Optics and Photonics **3**(2), 2011, pp. 128–160.

[4] SONG ZHANG, VAN DER WEIDE D., OLIVER J., *Superfast phase-shifting method for 3-D shape measurement*, Optics Express **18**(9), 2010, pp. 9684–9689.

[5] SHUANGYAN LEI, SONG ZHANG, *Flexible 3-D shape measurement using projector defocusing*, Optics Letters **34**(20), 2009, pp. 3080–3082.

[6] YING XU, EKSTRAND L., JUNFEI DAI, SONG ZHANG, *Phase error compensation for three-dimensional shape measurement with projector defocusing*, Applied Optics **50**(17), 2011, pp. 2572–2581.

[7] YAJUN WANG, SONG ZHANG, *Comparison of the squared binary, sinusoidal pulse width modulation, and optimal pulse width modulation methods for three-dimensional shape measurement with projector defocusing*, Applied Optics **51**(7), 2012, pp. 861–872.

[8] YAJUN WANG, SONG ZHANG, *Optimal pulse width modulation for sinusoidal fringe generation with projector defocusing*, Optics Letters **35**(24), 2010, pp. 4121–4123.

[9] AYUBI G.A., AYUBI J.A., DI MARTINO J.M., FERRARI J.A., *Pulse-width modulation in defocused three -dimensional fringe projection*, Optics Letters **35**(21), 2010, pp. 3682–3684.

[10] LOHRY W., SONG ZHANG, *3D shape measurement with 2D area modulated binary patterns*, Optics and Lasers in Engineering **50**(7), 2012, pp. 917–921.

[11] TAO XIAN, XIANYU SU, *Area modulation grating for sinusoidal structure illumination on phase -measuring profilometry*, Applied Optics **40**(8), 2001, pp. 1201–1206.

[12] ULICHNEY R., *Digital Halftoning*, MA: The MIT Press, Cambridge, 1997.

[13] PURGATHOFER W., TOBLER R.F., GEILER M., *Forced random dithering: improved threshold matrices foe ordered dithering*, [In] *IEEE International Conference Image Processing, 1994, Proceedings ICIP-94*, Vol. 2, 1994, pp. 1032–1035.

[14] BAYER B., *An optimum method for two-level rendition of continuous-tone pictures*, IEEE International Conference on Communications, Vol. 1, 1973, pp. 11–15.

[15] KNOX K.T., *Error diffusion: a theoretical view*, Proceedings of SPIE **1913**, 1993, pp. 326–331.

[16] YAJUN WANG, SONG ZHANG, *Three-dimensional shape measurement with binary dithered patterns*, Applied Optics **51**(27), 2012, pp. 6631–6636.

[17] LOHRY W., SONG ZHANG, *Genetic method to optimize binary dithering technique for high-quality fringe generation*, Optics Letters **38**(4), 2013, pp. 540–542.

[18] JUNFEI DAI, BEIWEN LI, SONG ZHANG, *High-quality fringe patterns generation using binary pattern optimization through symmetry and periodicity*, Optics and Lasers in Engineering **52**, 2014, pp. 195–200.

[19] JUNFEI DAI, SONG ZHANG, *Phase-optimized dithering technique for high-quality 3D shape measurement*, Optics and Lasers in Engineering **51**(6), 2013, pp. 790–795.

[20] JUNFEI DAI, BEIWEN LI, SONG ZHANG, *Intensity-optimized dithering technique for three-dimensional shape measurement with projector defocusing*, Optics and Lasers in Engineering **53**, 2014, pp. 79–85.

[21] SRINIVASAN V., LIU H.C., HALIOUA M., *Automated phase-measuring profilometry of 3-D diffuse objects*, Applied Optics **23**(18), 1984, pp. 3105–3108.
[22] SURREL Y., *Design of algorithms for phase measurements by the of phase stepping*, Applied Optics **35**(1), 1996, pp. 51–60.
[23] HUNTLEY J.M., SALDNER H., *Temporal phase-unwrapping algorithm for automated interferogram analysis*, Applied Optics **32**(17), 1993, pp. 3047–3052.

Received July 13, 2015
in revised form October 8, 2015